Energy & Environmental Science

Accepted Manuscript

ROYAL SOCIETY OF CHEMISTRY

www.rsc.org/ees

Journal Name

COMMUNICATION

Superior performance of borocarbonitrides, $B_xC_yN_z$, as stable, low–cost metal-free electrocatalysts for the hydrogen evolution reaction.

Received 00th January 20xx,
Accepted 00th January 20xx

DOI: 10.1039/x0xx00000x

www.rsc.org/

Manjeet Chhetri[a], Somak Maitra[a], Himanshu Chakraborty[b], Umesh V. Waghmare[b] and C. N. R. Rao*[a]

We report superior hydrogen evolution activity of metal-free borocarbonitrides (BCN) catalysts. The highly positive onset potential (-56 mV vs RHE) and the current density of 10 mA/cm^2 at an overpotential of 70 mV exhibited by a carbon-rich BCN with the composition BC_7N_2 demonstrates the extraordinary electrocatalytic activity at par with Pt. Theoretical studies throw light on the cause of high activity of this composition. The high activity and good stability of BCN surpass the characteristics of other metal-free catalysts reported in the recent literature.

Generation of hydrogen from water is potentially an important means of using solar energy for the benefit of mankind. The hydrogen evolution reaction (HER) is not only a vital part of electrochemical water splitting but also provides a way to understand the underlying mechanism of electron transfer processes in electrocatalysis. It is well known that platinum supported on carbon exhibits very good electrocatalytic HER activity[1-6]. Other transition metal catalysts have also been tried for HER[7-17], but it would be ideal to have a metal-free catalyst for the purpose, partly because of the scarcity and high cost of Pt[18]. Most of the photocatalysts and electrocatalysts reported so far suffer from low quantum efficiency as well as stability. A composite of carbon nitride (C_3N_4) and nitrogen-doped graphene (NG) has recently been reported to possess unique properties for successful electrocatalytic H_2 production[19]. Films of porous C_3N_4 layers with NG have also been shown to display excellent electrochemical HER performance with a high positive onset potential[20] and high exchange current density and stability comparable to platinum. The use of bimetallic core-shell electrocatalysts with carbonitrides for fuel cell applications has also been reported[21-23]. Other materials which have shown promising

Broader context

The use of hydrogen as a clean and efficient fuel has the potential of replacing scarce carbon based fuels. Using hydrogen as a fuel produces only water as the product thereby making it most suitable from environmental considerations. One of the ways to generate hydrogen is by the electrolysis of water by cathodically reducing hydrogen ions. However, hydrogen ion reduction is accompanied by a substantial overpotential unless an effective catalyst is used to reduce the gap between standard reduction potential of hydrogen ions and the overpotential. Pt or Pt group metals (PGM) have been extensively used for the hydrogen evolution reaction (HER) owing to their low overpotential and larger current density. However they suffer from the lack of inherent tolerance to catalyst poisons (like CO) and stability in the electrochemical environment. Furthermore, their high cost and limited availability are also drawbacks. Clearly there is need to replace Pt or PGM catalysts by less costly and easily synthesizable catalysts. In this context, non-precious metal catalysts specially carbon based materials have been under the limelight of research. We have found for the first time, borocarbonitrides (BCN) to be efficient HER electrocatalysts,with a carbon-rich sample exhibiting an onset potential of -56 mV (vs RHE) and a current density of 10 mA/cm^2 at an overpotential of 70 mV(vs RHE). The performance of the carbon-rich BCN found by us is superior to that reported for other non-metal electrocatalysts for HER. BCNs are low cost materials and have the potential to replace Pt based electrocatalysts.

[a] *New Chemistry Unit, International Centre for Materials Science, Jawaharlal Nehru Centre for Advanced Scientific Research, P.O Jakkur, Bangalore, 560064, India. Email: cnrrao@jncasr.ac.in*
[b] *Theoretical Sciences Unit, Jawaharlal Nehru Centre for Advanced Scientific Research, P.O Jakkur, Bangalore 560064, India.*
† Footnotes relating to the title and/or authors should appear here.
Electronic Supplementary Information (ESI) available: [Faradaic efficiency, Methods of First Principles calculations]. See DOI: 10.1039/x0xx00000x

Journal Name

COMMUNICATION

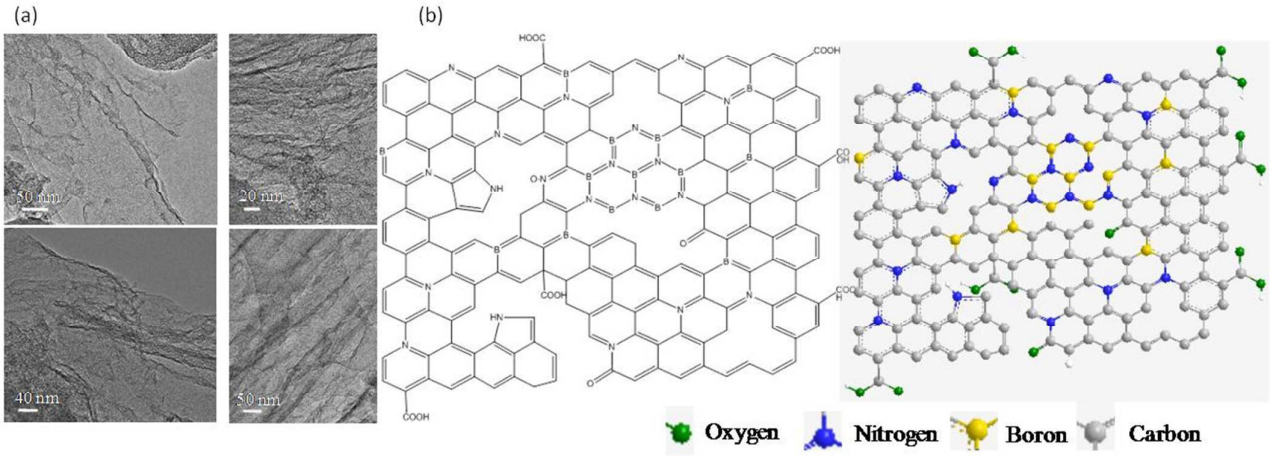

Fig.1: (a) TEM images of BCN-1 showing the sheet morphology. (b) Schematic of carbon rich BxCyNz sheets depicting the incorporation of B and N into the carbon network.

electrocatalytic HER activity are MoS_2 nanoparticles grown on graphene[24] and Mo_2C-carbon nanocomposites[25]. We considered it most appropriate to investigate the electrochemical HER activity of borocarbonitrides, $B_xC_yN_z$, which have been shown to have impressive surface and catalytic properties[26, 27] and are also low cost materials. These materials are nanoplatelets containing graphene and BN domains, possibly along with BCN rings[28-30]. They contain B-C, B-N, C-N, C-C bonds but no B-B and N-N bonds. They would have defect sites (e.g. sp^3-C, Stone-Wales defects) in the carbon network which can act as active sites (as nucleophile for H^+ ions) for electron transfer reactions. $B_xC_yN_z$ is different from B, N-codoped graphene in some ways such as thermal stability and presence of covalent BN domains in the carbon matrix. Although excess of BN domains impedes the electrochemical activity, the presence of it in trace amounts gives rise to $(BN)_x/C_y$ interface which is shown to have interesting adsorption properties. In this communication, we report the electrocatalytic activity of borocarbonitrides (designated as BCN in the text for simplicity) for HER. The high surface area and the low charge transfer resistance for electron transfer due to the presence of B and N atoms in the carbon network would be expected to reduce the overpotential for hydrogen production. To the best of our knowledge, there has been no report in the literature on the use of BCN as electrocatalysts for hydrogen production although they have been used for the oxygen reduction reaction (ORR)[31] .The present study demonstrates that carbon-rich BCN (BC_7N_2) exhibits outstanding electrocatalytic activity for HER. In order to understand the experimental results, we have carried out first-principles calculations which reveal the unique features of the highly active carbon-rich BCN.

We have prepared five compositions (BCN-1 to BCN-5) of borocarbonitrides, $B_xC_yN_z$ by the reaction of boric acid, urea and activated charcoal[28, 29]. Of these, BCN-1 is the most carbon rich sample with the composition of BC_7N_2 and BCN-5 has the least carbon content with the composition $BC_{1.1}N$ (see Table S1). Fig. 1 shows TEM images of the BCN sheets as well as a schematic depicting the structure and morphology. The surface areas obtained from N_2 adsorption isotherms show BCN-1 to have highest surface area (~1950 m^2/g) (Fig. S1) and BCN-4 having the lowest surface area of 1241 m^2/g. The presence of mesopores and micropores is indicated by the isotherms and pore size distribution. The pore diameter calculated by the DFT method is in the range of 3-19 nm and the pore volume in the range of 0.7 - 1.1 cm^3/g for all the

samples (see inset of Fig. S1). The Powder X-ray diffraction pattern

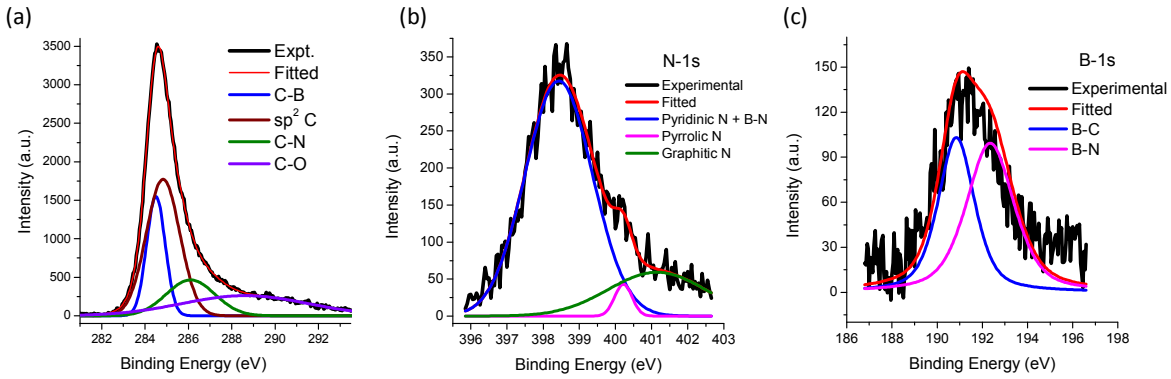

of BCN-1 shows broad peaks centered at 24.9° and 43.2° (2θ with

Fig. 2: (a) to (c)- X-ray photoelectron spectrum of BCN-1 showing core level spectrum of C, N and B respectively.

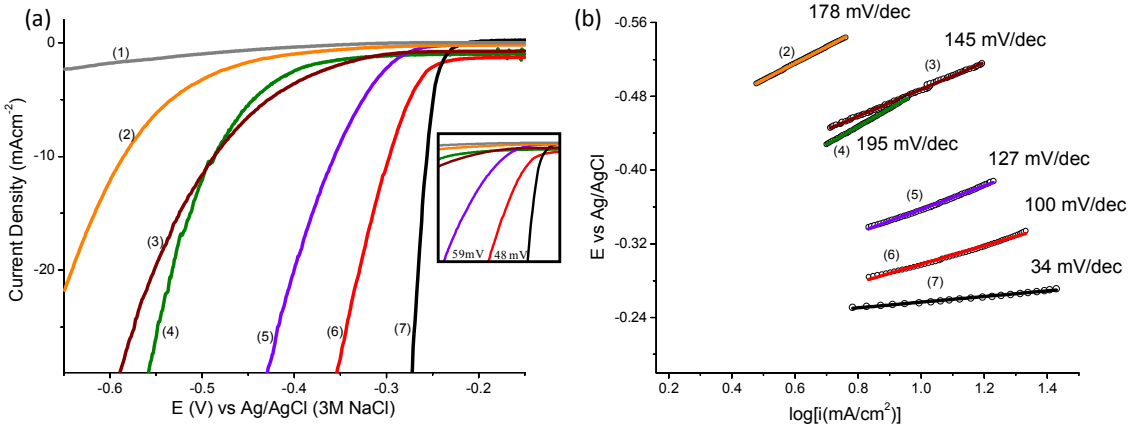

Fig. 3: HER electrocatalytic performance comparison (a) Linear Sweep Voltametry (LSV) comparison of all the $B_xC_yN_z$ samples including Pt/C and bare GCE. The inset compares the overpotential required to produce a current density of 10mA/cm^2 . (b) Tafel plots as deduced from the polarization curves in (a). The numbers within brackets in the figure respectively represent the following- (1) Bare GCE , (2) BCN-5, (3) BCN-4, (4) BCN-3, (5) BCN-2, (6) BCN-1, (7) Commercial 40% Pt/C)

FWHM of 6.8 and 3.5 respectively)(Fig. S2a), due to the (002) and (100) reflections, the broadening of peaks arising from the nanosized domains. Raman spectra show a prominent D-band (1335 cm^{-1}) due to defects along with the G-band (1590 cm^{-1}) and a weak 2D-band (2775 cm^{-1}) (see Fig. S2b). The BCN samples were free from metal impurities except for iron which is shown to be catalytically inactive (see ESI).

X-ray photoelectron spectroscopy (XPS) was employed to establish the nature of the chemical species in the BCN samples (see Fig. 2 for the spectra of BCN-1). Tables-S1 gives a summary of the compositions of the BCN samples. Core level spectra of the individual elements were deconvulated to obtain a detailed understanding of the bonding characteristics (see Fig. 2 and Fig. S2c). The B 1s signal consists of two peaks centered at 190.8 eV and 192.3 eV, which corresponds to the presence of B-C and B-N bonds respectively. The C-1s peak can be deconvulated

Journal Name

COMMUNICATION

Table 1: Electrochemical performance comparison of BCN samples and Pt/C

Sample	BET (m^2/g)	Onset [(a)] (mV)	η@10 mA/cm^2 [(a)], (mV)	η@20 mA/cm^2 [(a)], (mV)	Tafel Slope (mV/dec)	I_o (A/cm^2)	R_{ct} (ohm)	C_{dl} (mF/cm^2)
BCN-1	1950	-284	-298	-330	100	5.1×10^{-5}	13.6 Ω	0.108
BCN-2	1635	-314	-357	-401	127	3.2×10^{-5}	60.1 Ω	0.103
BCN-3	1470	-451	-487	-642	195	1.09×10^{-5}	64.3 Ω	0.033
BCN-4	1241	-444	-487	-533	145	9.1×10^{-6}	268.9 Ω	0.022
BCN-5	1580	-428	-586	-542	178	4.4×10^{-6}	384.6 Ω	0.020
Pt/C	--	-230	-250	-266	34	--	--	--

[a]Against RHE the values can be converted by adding 227.7 mV, following the equation, $E_{(RHE)} = E°_{(Ag/AgCl,\ 3\ M\ NaCl)} + E_{(Ag/AgCl,\ 3\ M\ NaCl)} + 0.059*pH$

Table 2: Comparison of electrochemical HER performance of BCN-1 with the recently reported non-precious metal catalysts.

Catalyst	Onset (mV) vs RHE	η@10 mA/cm^2 vs RHE	Tafel Slope (mV/dec)	Ref.
3D-MoS_2/N-GAs	-236	-261	230	32
N-MPG	-220	-239	109	33
C_3N_4@NG	-180	-240	51	19
N-Graphene on Si	-200	-260	74	34
g-C_3N_4nanoribbons	-80	-200	54	35
MoS_2/RGO	-100	-150	41	24
Defect rich MoS_2nanosheets	-120	-100	57	24
MoC_2/C nanocomposite	-100	-270[a]	110	25
40% Pt/C	2.3	22	34	This work
BC_7N_2	-56[b]	-70[b]	100	This work

[a]@ $5mA/cm^2$; [b]$E_{(RHE)} = E°_{(Ag/AgCl,\ 3M\ NaCl)} + E_{(Ag/AgCl)} + 0.059*pH$.

to four peaks at 284.4, 285.1, 285.9, 298.8 eV due to sp^2 carbon, C-B, C-N and C-O respectively. The deconvulation of the N-1s peak suggests the presence of different kinds of N-C bonds in BCN-1 (pyridinic, pyrollic and graphitic) as shown in Table S2. Thus the XPS analysis revealed the presence of B-C, B-N, C-N, C-C bonds in

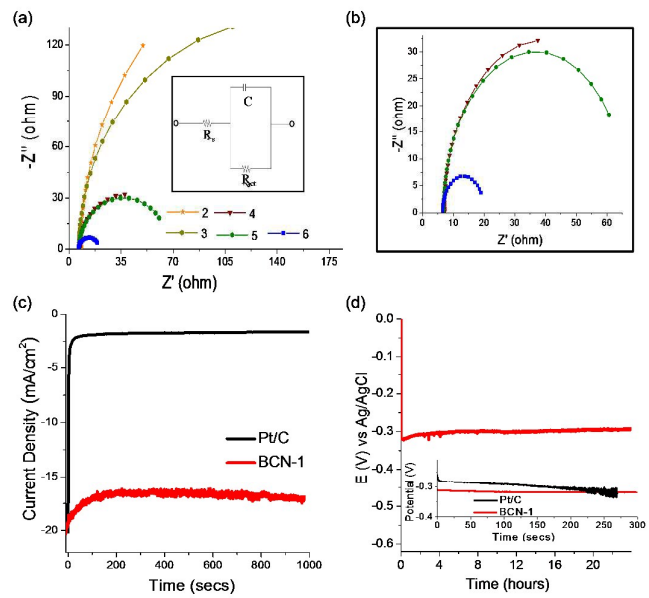

Fig. 4:Electrocatalytic performance testing of BxCyNz. (a) Nyquist plot of $B_xC_yN_z$ at the onset potential. (b) shows magnified image of (a) to show the same plot for low Rct value . (c) Activity retention test by amperometric i-t plot taken at -0.32 V for BCN-1 in comparison to Pt/C . (d) Chronopotentiometry plot to produce a current density of 20mA/cm2 . Inset shows the comparative plot for BCN-1 and Pt/C . The letters in (a) represents the same as in figure 3.

BCN samples suggesting the presence of graphene and BN (as depicted in scheme Fig. 1b). Table S3 gives the percentages of B-C and B-N bonds on the surface of the BCN samples. We have also analyzed the O-1s signal (see ESI). EDAX and CHN elemental analysis gave results which corresponded well with the compositions obtained from XPS.

Electrochemical performance of the BCN samples for HER was investigated by Linear Sweep Voltametry (LSV) at 1600 rpm and 5 mV/s scan rate with deaerated 0.5 M H_2SO_4 as the electrolyte. The cathodic polarization curves of all the samples are shown in Fig. 3a. For purpose of comparison, data on 40% Pt/C and bare (GCE) is also included. GCE exhibits almost null activity in comparison with BCN and Pt/C polarization curves. The onset potential for HER was found to be -0.28 V (Ag/AgCl) whereas that for Pt/C was -0.23 V (Ag/AgCl). The value of the overpotential (η) gives an idea of the extent of polarization upon the passage of faradaic current (in this case due to H_2 evolution), a lower η signifying better catalytic activity generating more H_2 on application of smaller cathodic potential. The values of η at 10 and 20mA/cm^2 are -298 mV and -330 mV signifying the rapid rate of electron transfer on BCN-1 (see Table 1). The inset in Fig. 3a shows the difference in the overpotential required to produce a current density of 10mA/cm^2 for the BCN samples and the Pt/C. In comparison with the recently reported non-precious metal catalysts, BCN-1 shows markedly better performance for HER (Table 2). For the ease in comparison, the potentials reported in Table 1 are against Reversible Hydrogen Electrode (RHE) obtained through RHE calibration using the equation[36], $E_{(RHE)} = E°_{(Ag/AgCl,\ 3M\ NaCl)} + E_{(Ag/AgCl)} + 0.059\ pH$.

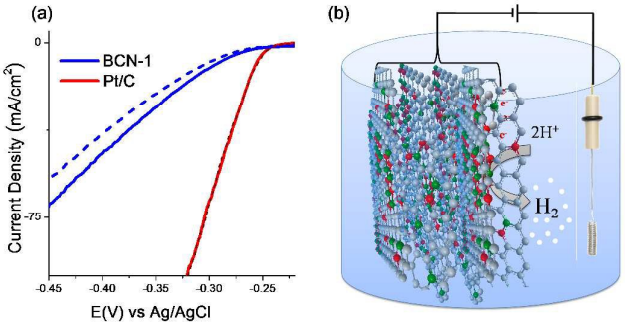

Fig. 5: (a) LSV plot before and after 1000 cycles (between -0.35 v to 0.1 V) for both BCN-1 and Pt/C. (b) Schematic showing the HER activity of $B_xC_yN_z$ sheets.

The high HER activity of BCN nanosheets is further manifested by the Tafel plots (Fig. 3b) and the corresponding mechanism for H_2 generation (See supporting information). The Tafel equation can be deduced from the Butler-Volmer equation and the final form of the equation is given by equation-1,

$$\eta = a + b\log\left(\frac{i}{i_o}\right) \quad (1)$$

where η is the overpotential, i and i_o are respectively the current density and the exchange current density, 'b' is the tafel slope and 'a' is the constant (see supporting information for details). We found that the hydrogen evolution by BCN samples follow Volmer mechanism[37] giving a tafel slope of 100mV/dec (Fig. 3b). In order to

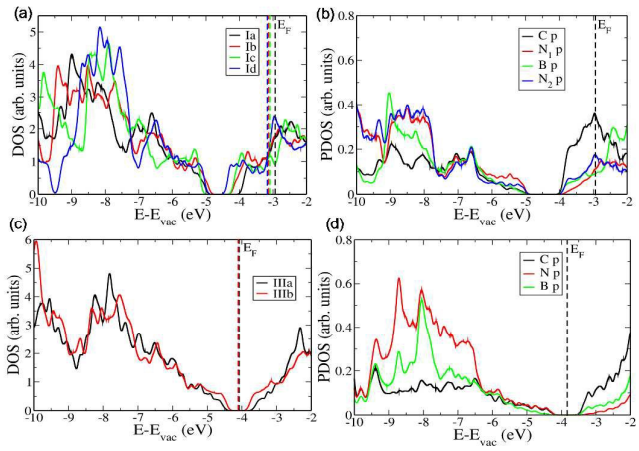

Fig 6: (a) DOS for four configurations of BC_7N_2 (I), (b) PDOS of its first configuration (Ia), (c) DOS for two configurations of BC_8N (III) and (d) PDOS of $B_2C_2N_2$ (II). See Fig. S5 for different configurations.

probe the interfacial property of the BCN samples and the ease of electrical exchange between the solution and the electrode, Electrochemical Impedance Spectroscopy was performed at the onset potential of the sample from 10^5 to 1 Hz with an AC voltage of 5 mV. Figures 4a and b show the Nyquist plots for the samples. BCN-1 shows a minimum charge transfer resistance (R_{ct}) of 13.6 Ω. Lower R_{ct} reveals that faster electron transfer rate between BCN and the GCE and the electrolyte resulting in acceleration of HER kinetics. This is also corroborated from the polarization curves and the Tafel slope values. For the determination of the Faradaic efficiency (FE) of HER catalysed by BC_7N_2, we measured the amount of H_2 produced by electrolysis for 2 hours. The measured value matches well with the calculated value (assuming 100% efficiency) (see Fig. S6)

To confirm the high activity and lower charge transfer resistance we have compared the electrochemical active surface areas of the samples by calculating the double layer capacitance (see supporting information for detailed calculations). The value of C_{dl} is 0.108mF/cm^2 for BCN-1, which is the highest value amongst all the BCN samples (Fig. S3 and Table 1). Since double layer capacitance is directly proportional to the electrochemical active surface area for carbon based materials, the values obtained for BCN-1 correspond

to an enhancement factor of one order of magnitude relative to the other samples (Table 1). The higher activity with lower R_{ct} for BCN-1 is due to the high electrical conductivity owing to the higher proportion of carbon in the network[29] and the larger active surface area. It is noteworthy that the electronic structure and properties which enhance electron transfer reactions are related to the composition and the relative ordering of graphene and BN domains. BCN-1 has a high B-C:B-N ratio of 6.7 (Table S3) leading to lower proportion of BN domains. Furthermore graphitic N-C interaction would favour defect sites which play a key role in electron transfer reactions. The samples obtained from the controlled experiments without urea and boric acid respectively show that singly doped carbon (with N and B) does not show enhanced HER activity.

Stability is an important parameter of catalyst activity. We have employed chronoamperometry (CA), chronopotentiometry (CP) (Figures 4c and d) and cyclic voltametric (CV) to test the % retention of the electrochemical activity as a function of time or cycles. CA was performed at -0.32 V (Ag/AgCl, 3 M NaCl) and CP was done at a current density of 20mA/cm^2. Samples were also potentially swiped between 0.1 V and -0.35 V and after the cycling, LSV was again taken to compare. BCN-1 shows exceptional stability in comparison to Pt/C catalyst whereby ~80% of the activity is retained in comparison to Pt/C (only ~10 % activity retention) in 1000 seconds (Figures 4c and S4) to obtain current at -0.32 V. From the CP study, (see inset of Fig. 4d), BCN-1 shows activity at par with Pt/C to produce a current density of 20mA/cm^2. We have performed CP for 24 hours (Fig. 4d) and found BCN-1 to be a highly stable catalyst for HER. To reinforce these conclusions, we have performed CV in the potential window of -0.35 V to 0.1 V for 1000 cycles, recording the polarization curves before and after the cycling (Fig. 5a). We observe ~83% retention in activity as also seen from the chronoamperometric i-t (CA) test (Fig. S3). The degradation of graphitic carbon in acidic medium is negligible and the possible loss of active surface area is less than that for Pt/C (catalyst detachment, agglomeration, carbon corrosion etc).

In our first principles calculations, we have examined the electronic density of states (DOS) and the partial density of states (PDOS) of the three compositions, BC_7N_2 (I), $B_2C_2N_2$ (II) and BC_8N (III), by shifting the energy suitably to have vacuum level at 0 eV. For all the configurations of BC_7N_2 (Fig. S5), Fermi energy (E_F) is around -3.2 eV, which gives an overpotential of about 1.2 eV relative to the redox potential of HER. Secondly, it is in a conduction band separated by a gap of about 0.5 eV from the valence band giving n-type carriers at relatively high density, highest for the configuration Ia (Fig. 6). The bottom of the conduction band is just above the HER potential. From the PDOS, it is clear that these states are contributed largely by *p* orbitals of C and N atoms, and reflect that the two substituted N atoms have different chemical character. Visualization of the frontier occupied state of the lowest energy configurations reveals C-C and C-N bonds are relevant to the electrocatalytic activity. The electronic structures of both BC_8N and $B_2C_2N_2$(Fig. 6c and 6d) exhibit a gap of about 0.5 eV, and the top of the valence band (with fairly low density of states) is just above or barely touches the redox potential of the HER, consistent with low

Fig 7: Bandgaps and valence (black) and conduction (red) band edge positions of the

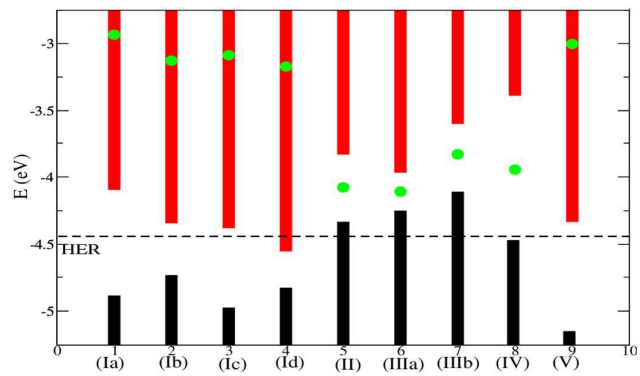

different configurations. The energy level for hydrogen evolution reaction (HER) is denoted by dotted line and their Fermi energies by green circles. Here, IV and V refer to $B_2C_6N_2$ and $B_2C_5N_3$ (see supporting information for configurations).

electrocatalytic activity. Their frontier occupied states involve mainly C-C bonds while the valence and conduction band edges of the configurations of BC_7N_2 (Ia, Ib and Ic) straddle the HER redox potential (-4.44 eV), those of BC_8N and $B_2C_2N_2$ do not (Fig. 7 and Table S4). A Comparative study of the electronic structures of C_8N_2 and BC_7N_2 reveals that the electrostatic balance provided by the B atom is essential to get stability and optimal alignment of the electronic structure with respect to the HER potential (see Fig. S9). We have examined around 60 configurations for the interaction between H_2O and BC_7N_2 (including van der Waals interactions, see Fig S10). We find that the energy of adsorption of H_2O with the 1a configuration spans the widest range from 11 - 26 kJ mol^{-1} among all the configurations of BC_7N_2 (see Fig. S11). Moreover, the electric dipoles of H_2O and the N-B-N structural motifs of 1a

configuration couple with each other and with the external electric field, an aspect of relevance to the electrocatalytic properties. While all the four chemically ordered states of BC_7N_2 are comparable in their electronic properties, our results indicate that 1a may be more optimal for electrocatalysis in HER. Thus, out of the four configurations, Ia, where both N atoms are bonded to B atoms is the best candidate as an electrocatalyst for hydrogen generation. We also include a comparative analysis of the electronic structure of $B_2C_5N_3$ containing carbon nitride rings, and BC_7N_2 with assessment of their activity towards HER (see Fig. S12). Electronic DOS of $B_2C_5N_3$ and BC_7N_2 are qualitatively similar, but with a lower over potential of the former for HER, with the conduction band edge above the HER by ~ 0.25 eV. $B_2C_5N_3$ with CN- rings is indeed suitable for catalysis of HER and water splitting (see Fig. S12 bottom), However, a comparison of the energies of $B_2C_5N_3$ and $B_2C_6N_2$ relative to graphene, boronitride and BC_7N_2 shows that the two structures are energetically not favorable, with $B_2C_5N_3$ less stable than $B_2C_6N_2$. BCN containing carbon-nitride rings is energetically less favorable than BC_7N_2.

Conclusions

We have successfully demonstrated the efficacy of borocarbonitride sheets as an excellent low-cost, metal-free (see ESI for the analysis) catalyst for hydrogen generation (Fig. 5b). This is the first report on the use of BCN as HER catalysts. Amongst all the BCN samples, carbon-rich BCN-1 shows the best activity with a performance superior to that of other non-precious metal electrocatalyst (Table 2). The onset potential of -0.28 V (vs Ag/AgCl) is close to that of Pt (-0.23 V). BCN-1 also exhibits stability upto 24 hours requiring an overpotential of -0.32 V (vs Ag/AgCl) to produce a current density of 20mA/cm^2. It is noteworthy that BCN-1 contains a larger proportion of pyridinic than pyrollic nitrogens and a high percentage of B-C bonds, the low proportion of BN bonds also contributing to higher conductivity. Our theoretical studies show that substitution of B and N in equal concentrations opens up a gap, with the valence band unfavourably located relative to the HER potential. Substitution of excess N results in the population of the conduction bands with electrons and shifts the valence and conduction bands to lower energy and favours the alignment of bands to facilitate electrocatalysis. We believe that with compositional and morphological modifications, the electrochemical activity of BCN can be further improved.

Acknowledgements

MC thanks UGC, India for JRF and JNCASR for the advanced facilities. U.V.W. & H.C. acknowledge discussions and interactions with M. L. Klein and support through the Centre for the Computational Design of Functional Layered Materials, an Energy Frontier Research Centre funded by the U.S. Department of Energy, Office of Science, Basic Energy Sciences under Award No. DE-SC0012575. We also acknowledge S. Sampath, Indian Institute of Science for the help in Faradaic efficiency measurements.

Notes and References:

1. J. K. Norskov, T. Bligaard, J. Rossmeisl and C. H. Christensen, *Nature Chemistry*, 2009, **1**, 37-46.
2. K. Neyerlin, W. Gu, J. Jorne and H. A. Gasteiger, *J. Electrochem. Soc.*, 2007, **154**, B631-B635.
3. S. A. Grigoriev, P. Millet and V. N. Fateev, *J. Power Sources*, 2008, **177**, 281-285.
4. P. Millet, R. Ngameni, S. A. Grigoriev, N. Mbemba, F. Brisset, A. Ranjbari and C. Etiévant, *Int. J. Hydrogen Energy*, 2010, **35**, 5043-5052.
5. D. V. Esposito, S. T. Hunt, A. L. Stottlemyer, K. D. Dobson, B. E. McCandless, R. W. Birkmire and J. G. Chen, *Angew. Chem. Int. Ed.*, 2010, **122**, 10055-10058.
6. N. M. Marković, B. N. Grgur and P. N. Ross, *J. Phys. Chem. B*, 1997, **101**, 5405-5413.
7. S. Bai, C. Wang, M. Deng, M. Gong, Y. Bai, J. Jiang and Y. Xiong, *Angew. Chem. Int. Ed.*, 2014, **53**, 12120-12124.
8. E. J. Popczun, J. R. McKone, C. G. Read, A. J. Biacchi, A. M. Wiltrout, N. S. Lewis and R. E. Schaak, *J. Am. Chem. Soc.*, 2013, **135**, 9267-9270.
9. D. Brown, M. Mahmood, A. Turner, S. Hall and P. Fogarty, *Int. J. Hydrogen Energy*, 1982, **7**, 405-410.
10. D. Brown, M. Mahmood, M. Man and A. Turner, *Electrochim. Acta*, 1984, **29**, 1551-1556.
11. C. Fan, D. Piron, A. Sleb and P. Paradis, *J. Electrochem. Soc.*, 1994, **141**, 382-387.
12. I. A. Raj and K. Vasu, *J. Appl. Electrochem.*, 1990, **20**, 32-38.
13. M. Wang, L. Chen and L. Sun, *Energy Environ. Sci.*, 2012, **5**, 6763-6778.
14. J.-F. Capon, F. Gloaguen, F. Y. Pétillon, P. Schollhammer and J. Talarmin, *Coord. Chem. Rev.*, 2009, **253**, 1476-1494.
15. V. Artero, M. Chavarot-Kerlidou and M. Fontecave, *Angew. Chem. Int. Ed.*, 2011, **50**, 7238-7266.
16. D. L. DuBois and R. M. Bullock, *Eur. J. Inorg. Chem.*, 2011, **2011**, 1017-1027.
17. X. Fan, Z. Peng, R. Ye, H. Zhou and X. Guo, *ACS Nano*, 2015, **9**, 7407-7418.
18. H. Vrubel and X. Hu, *Angew. Chem.*, 2012, **124**, 12875-12878.
19. Y. Zheng, Y. Jiao, Y. Zhu, L. H. Li, Y. Han, Y. Chen, A. Du, M. Jaroniec and S. Z. Qiao, *Nat. Commun.*, 2014, **5**.

20. J. Duan, S. Chen, M. Jaroniec and S. Z. Qiao, *ACS Nano*, 2015, **9**, 931-940.
21. V. Di Noto, E. Negro, S. Polizzi, F. Agresti and G. A. Giffin, *ChemSusChem*, 2012, **5**, 2451-2459.
22. V. Di Noto, E. Negro, S. Polizzi, K. Vezzù, L. Toniolo and G. Cavinato, *Int. J. Hydrogen Energy*, 2014, **39**, 2812-2827.
23. E. Negro, S. Polizzi, K. Vezzù, L. Toniolo, G. Cavinato and V. Di Noto, *Int. J. Hydrogen Energy*, 2014, **39**, 2828-2841.
24. Y. Li, H. Wang, L. Xie, Y. Liang, G. Hong and H. Dai, *J. Am. Chem. Soc.*, 2011, **133**, 7296-7299.
25. N. S. Alhajri, D. H. Anjum and K. Takanabe, *J. Mater. Chem. A*, 2014, **2**, 10548-10556.
26. S. Sen, K. Moses, A. J. Bhattacharyya and C. N. R. Rao, *Chem. Asian J.*, 2014, **9**, 100-103.
27. K. Raidongia, A. Nag, K. P. S. S. Hembram, U. V. Waghmare, R. Datta and C. N. R. Rao, *Chem. Euro. J.*, 2010, **16**, 149-157.
28. N. Kumar, K. Moses, K. Pramoda, S. N. Shirodkar, A. K. Mishra, U. V. Waghmare, A. Sundaresan and C. N. R. Rao, *J. Mater. Chem. A*, 2013, **1**, 5806-5821.
29. M. Kota, N. S. Sharmila, U. V. Waghmare and C. N. R. Rao, *Mater. Res. Express*, 2014, **1**, 025603.
30. C. N. R. Rao, K. Gopalakrishnan and U. Maitra, *ACS Appl. Mater. Interfaces*, 2015, **7**, 7809-7832.
31. K. Moses, V. Kiran, S. Sampath and C. N. R. Rao, *Chem. Asian J.*, 2014, **9**, 838-843.
32. Y. Hou, B. Zhang, Z. Wen, S. Cui, X. Guo, Z. He and J. Chen, *J. Mater. Chem. A*, 2014, **2**, 13795-13800.
33. X. Huang, Y. Zhao, Z. Ao and G. Wang, *Sci. Rep.*, 2014, **4**.
34. U. Sim, T.-Y. Yang, J. Moon, J. An, J. Hwang, J.-H. Seo, J. Lee, K. Y. Kim, J. Lee, S. Han, B. H. Hong and K. T. Nam, *Energy Environ. Sci.*, 2013, **6**, 3658-3664.
35. Y. Zhao, F. Zhao, X. Wang, C. Xu, Z. Zhang, G. Shi and L. Qu, *Angew. Chem. Int. Ed.*, 2014, **53**, 13934-13939.
36. J. Guo, F. Li, Y. Sun, X. Zhang and L. Tang, *J. Power Sources*, 2015, **291**, 195-200.
37. C. G. Morales-Guio, L.-A. Stern and X. Hu, *Chem. Soc. Rev.*, 2014, **43**, 6555-6569.